Quantum Dynamics of the $CH_4 + H \rightarrow CH_3 + H_2$ Reaction: Full-Dimensional and Reduced Dimensionality Rate Constant Calculations†

Fermín Huarte-Larrañaga and Uwe Manthe*

Theoretische Chemie, Technische Universität München, Lichtenbergstrasse 4, Garching D-85747, Germany

Received: September 29, 2000; In Final Form: November 27, 2000

Quantum mechanical calculations for the thermal rate constant of the combustion related reaction, $CH_4 + H \rightarrow CH_3 + H_2$, are reported. Benchmark full-dimensional results are given and compared to those derived from classical transition state theory as well as to some published reduced dimensionality results. The role played by some of the different degrees of freedom in the reactive process is investigated by comparing additional reduced dimensionality results to the exact ones. This proves valuable for the development of possible strategies to study involved reactive processes.

I. Introduction

Among the chemist main duties there is the task of understanding, and therefore accurately describing, chemical reactions. The deepening in the chemical process nature is achieved by both the accurate study of reactions and the development of approximate strategies which allow the undertaking of more involved (and realistic) systems. Therefore, the development of approximate approaches for the quantum mechanical description of elementary processes involving small systems in the gas phase is of great importance. On the other hand, it is also necessary to have at hand accurate quantum mechanical results which will validate or not these approximate strategies on systems of moderate complexity. In this sense, while the accurate description of three and four-atomic processes at a full quantum mechanical level seems nowadays feasible, the step toward bigger systems has only been achieved through simplified models. No accurate full-dimensional study had been yet reported for a system containing more than four atoms. In a recent communication,[1] we presented, for the first time, fully converged results for the quantum mechanical calculation of the title reaction's rate constant considering all its 12 internal degrees of freedom. In this paper, we intend to extend the presentation of said results as well as some other approximate results, obtained treating accurately only some particular degrees of freedom, which will help to deepen in the understanding of this chemical process characteristics.

Combustion related reactions are regarded as a family of processes of high technological interest. Among them, the hydrogen abstraction from methane is seen lately as a suitable prototype for the theoretical study of bimolecular reactions due to its relatively small size, which enables fairly accurate ab initio calculations. Thus, several theoretical and experimental studies can be found in the literature for the family of reactions given by $CH_4 + X \rightarrow CH_3 + HX$, where X is Cl, O, or H. In this work we will be concerned with the hydrogen abstraction from methane by a colliding hydrogen atom. An extensive experimental background on this process can be found in the literature. The first experimental rate coefficients were published already in 1954,[2] and several studies have been carried out afterward, most recently reviewed by Baulch et al.[3] After this review, new experimental rate constant results have been published for both the title reaction[4,5] and its reverse.[6] Most recently, Momose et al.[7] have published their experiments on the reverse title reaction at 5 K in solid parahydrogen in which they found an interesting isotope effect. In contrast to such an abundant experimental background, not until the 1980s were the first theoretical works published by Walch[8] and Schatz, Wagner and Dunning.[9] Prior to this, semiempirical surfaces had been published in the 1970s by Bunker and co-workers[10−12] and Raff.[13] In a later work, Truhlar and co-workers[14] analyzed the two potential energy surfaces employing ab initio calculations and reaction-path methods and concluded that Raff's potential surface was physically more reasonable, although not accurate enough to allow quantitative dynamics studies. Resulting from this study a new fit[15] was developed, on the basis of Raff's functional, but calibrated to kinetic data and ab initio results by Duchovic, Hase, and Schlegel.[16] On this surface, the authors[15] performed variational transition state theory and semiclassical tunneling calculations. However, the surface developed by Joseph, Steckler, and Truhlar[15] is not only specified in terms of the incoming hydrogen atom but also in terms of the abstracted atom and therefore it is not symmetric concerning the four methane hydrogen atoms. To run trajectory calculations, Jordan and Gilbert[17] used the Joseph[15] potential as a basis for constructing a new potential energy function which would be symmetric for all four methane hydrogen atoms. This has been the potential energy functional used in this work and other previous reduced dimensionality studies published by Takayanagi,[18] Yu, and Nyman,[19] and Wang, Li, Zhang, and Zhang.[20] We have recently presented[1] our first results on this surface. Here we intend to deepen in the study of the reactive system including the results obtained by carrying out several reduced dimensionality calculations and comparing them to the full-dimensional ones in order to estimate the role that the different internal degrees of freedom play in the reaction.

II. Theory

Probably the main intrinsic feature characterizing any reactive process is its rate constant. Whenever a process occurs via a potential energy barrier, it is well-known that its rate constant

† Part of the special issue "William H. Miller Festschrift".

* To whom correspondence should be addressed. E-mail: uwe.manthe@ch.tum.de.

10.1021/jp003579w CCC: $20.00
Published on Web 01/17/2001

is determined by the dynamics occurring in the vicinity of this barrier, while dynamics in the outer regions simply determines the specific state to state transitions. Flux correlation functions have proven to be a powerful theoretical tool for the direct calculation of reaction rate constants by examining the dynamics only in the strong interaction region of the potential energy surface. Unlike full scattering calculations, this approach must not examine the whole configurational space until the very asymptotic region. This feature shows up as a crucial advantage to undertake large systems, such as the title system, when compared to full scattering calculations. Theory for the method employed in this work has been extensively detailed elsewhere,[21−29] and therefore, only its general ideas will be given here.

The rate constant of a chemical reaction can be calculated directly, as shown by Miller,[21] as a time integral of the flux−flux correlation function $C_f(t)$,

$$k(T) = \frac{1}{Q_r(T)}\int_0^\infty dt\, C_f(t) \tag{1}$$

$$C_f(t) = tr(\hat{F}e^{i\hat{H}t/\hbar - \hat{H}/2kT}\hat{F}e^{-i\hat{H}t/\hbar - \hat{H}/2kT}) \tag{2}$$

where $Q_r(T)$ is the reactant's partition function, $\hat{H}$ is the full Hamiltonian, $\hat{F} = i/\hbar[\hat{H},h]$ is the symmetrized flux operator, and h is a Heaviside function discriminating products from reactants. In another work, Miller, Schwartz, and Tromp[22] showed that eq 1 can be rewritten in an energy-dependent form as

$$k(T) = \frac{1}{2\pi Q_r(T)\hbar}\int_0^\infty dE e^{-E/kT}N(E) \tag{3}$$

where the cumulative reaction probability $N(E)$ can be expressed as

$$N(E) = 2\pi^2\hbar^2 tr(\hat{F}\delta(\hat{H} - E)\hat{F}\delta(\hat{H} - E)) \tag{4}$$

Introducing a reference temperature to regularize the flux operator, the so-called thermal flux operator is obtained (see ref 23),

$$\hat{F}_{T_0} = e^{-\hat{H}/2kT_0}\hat{F}e^{-\hat{H}/2kT_0} \tag{5}$$

and eqs 3 and 4 can then be written as

$$k(T) = \frac{1}{2\pi Q_r(T)\hbar}\int_0^\infty dE\, e^{-E(1/kT - 1/kT_0)}N_{T_0}(E) \tag{6}$$

$$N_{T_0}(E) = 2\pi^2\hbar^2 tr(\hat{F}_{2T_0}\delta(\hat{H} - E)\hat{F}_{2T_0}\delta(\hat{H} - E)) \tag{7}$$

Employing the spectral decomposition of the thermal flux operator, eq 7 can be written in terms of the thermal flux eigenstates:

$$N_{T_0}(E) = 2\pi^2\hbar^2\sum_{l,m} f_l f_m |\langle f_l|\delta(\hat{H} - E)|f_m\rangle|^2 \tag{8}$$

Here f_m and $|f_m\rangle$ denote the eigenvalues and eigenstates of the thermal flux operator, respectively. These thermal flux eigenstates can be seen as vibrational states of the activated complex.[24,25] The thermal flux operator has only few nonvanishing eigenvalues and these can therefore be quite efficiently calculated by means of a Lanczos-type diagonalization scheme. Upon Fourier transforming eq 8, one obtains

$$N_{T_0}(E) = \pi\sum_{l,m} f_l f_m \left|\frac{1}{\sqrt{2\pi}}\int_{-\infty}^{\infty} dt\, e^{iEt/\hbar}\langle f_l|e^{-i\hat{H}t/\hbar}|f_m\rangle\right|^2 \tag{9}$$

and only the time propagation of the thermal flux eigenstates remains prior to the evaluation of the above integral and the cumulative reaction probability is obtained.

The multiconfigurational time dependent Hartree (MCTDH) approach[26,27] has been employed in the present calculations for the time propagation of the wave function. This scheme proves to be efficient for short time multidimensional problems. Let us recall the particular expression of the wave function in the MCTDH approach for a system with f degrees of freedom:

$$\psi(x_1,...,x_f,t) = \sum_{j_1=1}^{n_1}...\sum_{j_f=1}^{n_f} A_{j_1...j_f}(t)\phi_{j_1}^{(1)}(x_1,t)...\phi_{j_f}^{(f)}(x_f,t) \tag{10}$$

where $A_{j_1..j_f}$ are the expansion coefficients and the $\phi_{j_i}^{(i)}(x_f,t)$ denote the so-called time-dependent single-particle functions. In words, the wave function is expanded on a direct product basis set of single variable time-dependent functions, called single particle functions. The equations of motion which guarantee the optimal choice of these single particle functions are derived from the Dirac-Frenkel variational principle. To make the MCTDH scheme suitable to the above approach for the calculation of the rate constants, some specific modifications of the Lanczos diagonalization scheme[28] and the CDVR scheme[29] for the evaluation of the potential energy matrix representation elements are required.

III. Numerical Calculation

The potential energy surface employed in this work has been the one developed by Jordan and Gilbert.[17] This surface shows a C_{3v} transition state geometry with the abstracting hydrogen atom, the abstracted hydrogen atom, and the carbon atom lying on the C_3 symmetry axis. The process, on this surface, is 0.12 eV endoergic (0.001 eV exoergic if zero point energy is included) and the barrier to reaction rises 0.474 eV above the reactants asymptote (0.437 eV, vibrationally adiabatic).

As described in the Introduction, the potential energy functional was developed starting from a surface fit by Joseph, Steckler, and Truhlar[15] who, employed a functional originally developed by Raff.[13] The motivation for Jordan and Gilbert to develop a new fit was essentially to symmetrize the surface which, as formulated in ref 15, was not symmetric with respect to all methane hydrogen atoms. Obviously, for a system such as the title one, a 5-fold symmetric functional would be desirable but, taking into account that this would complicate remarkably the form of the functional and that one is usually considering energies well below the exchange process, a 4-fold symmetric potential energy ought to be sufficient to describe the reaction. This task was performed by Jordan and Gilbert.[17] However, as it has been pointed out by Espinosa-García and García-Bernáldez[30] and ourselves,[1] the functional is, as published, not completely symmetric with respect to the permutation of the methane hydrogens. In particular, the asymmetry arises from the expression of the force constant in the out of plane bending term (for a better understanding of the term see ref 17):

$$\Delta_{ij} = \cos^{-1}\left(\frac{(\mathbf{r}_j - \mathbf{r}_l)\times(\mathbf{r}_j - \mathbf{r}_k)}{|(\mathbf{r}_j - \mathbf{r}_l)\times(\mathbf{r}_j - \mathbf{r}_k)|}\cdot\frac{\mathbf{r}_i}{|\mathbf{r}_i|}\right) - \Theta_{ij} \tag{11}$$

where suffixes label the different methane hydrogen atoms, r_α stands for the corresponding C − H_α internuclear vector, and

TABLE 1: Calculated Transition State normal Mode Frequencies

	ω/cm^{-1}
Q_1	1094i
$Q_{2,3}$	587
Q_4	1204
$Q_{5,6}$	1245
$Q_{7,8}$	1439
Q_9	1601
Q_{10}	2963
$Q_{11,12}$	3097

Θ is a reference angle (for further detail see ref 17). In their work,[17] the authors indicate that attention should be paid so that the set $\{\mathbf{r}_j, \mathbf{r}_k, \mathbf{r}_l\}$ is right-handed. This, however, as pointed out in ref 30, is sensitive to the order in which the hydrogen atoms are labeled and, therefore, not fully symmetric. After thorough inspection of the functional, we came to the conclusion that it should the set $\{\mathbf{r}_i, \mathbf{r}_j, \mathbf{r}_k\}$ to be right-handed.

Transition state normal coordinates were chosen for the description of the system during the calculation. Such coordinates should minimize correlation effects in the transition state region and, thus, facilitate the efficient performance of the MCTDH approach. Normal modes and normal coordinates were calculated at the transition state geometry and the corresponding linear transformation matrix was used throughout the calculation to convert the working coordinates into Cartesian coordinates. Mixed derivatives in the kinetic energy resulting from vibrational angular momentum have been considered to be irrelevant since the moments of inertia proved not to change significantly within the range of relevant geometries on the time scale investigated. From the normal coordinate analysis, the following 12 normal vibrational modes were obtained: the imaginary mode (Q_1) which was employed as reaction coordinate, a doubly degenerate low-frequency bending mode ($Q_{2,3}$), an umbrella mode (Q_4), a doubly degenerate high-frequency bend ($Q_{5,6}$), another doubly degenerate bending mode essentially involving the motion of the hydrogens which are not being abstracted ($Q_{7,8}$), a symmetric stretch along the C_3 symmetry axis (Q_9) concerning the collinear internal motion of the H−H−CH$_3$ fragments, and a symmetric and doubly degenerate asymmetric stretches concerning, again, mainly the methyl fragment (Q_{10} and $Q_{11,12}$). Corresponding frequencies can be found in Table 1. To find out which were the normal modes mostly involved in the reactive process, the potential energy surface was mapped onto several two-dimensional contour plots. From them, it was seen that the coordinates mainly participating in the reactive event were those corresponding to the imaginary frequency, the umbrella mode and the symmetric stretch, namely Q_1, Q_4, and Q_9, although the role played by the other modes is by no means negligible, as it will be seen later in the article. The use of a MCTDH scheme for expressing the wave function in the method requires the dividing surface, where the flux is calculated, to be a single variable function. Although in principle, the numerically converged result will be independent of the choice for the dividing surface, from inspection of the potential energy contour plots, and some test calculations it was found that the best dividing surface would be obtained by linearly combining Q_1 and Q_9. Thus, transformed coordinates $Q'_1 = \sin\alpha\, Q_1 + \cos\alpha\, Q_9$ and $Q'_9 = \cos\alpha\, Q_1 - \sin\alpha\, Q_9$ with $\alpha = 55°$ were employed and the dividing surface was located at $Q'_1 = 0$.

Convergence parameters for the representation of the wave function are shown in Table 2. In this table, the time-dependent basis size (i.e., number of single particle functions) n_i, employed for each coordinate can be found, together with the method through which these time-dependent functions are generated

TABLE 2: Converged Parameters for the Calculation[a]

coordinate	n_i	scheme	basis	grid range [au]
Q'_1	6	FFT	48	−100,140
Q_2,Q_3	3	DVR	15	
Q_4	3	FFT	32	−100,100
Q_5,Q_6	3	DVR	10	
Q_7,Q_8	2	DVR	6	
Q'_9	5	FFT	48	−155,85
Q_{10}	2	DVR	8	
Q_{11},Q_{12}	2	DVR	8	

[a] n_i stands for single particle function, "scheme" stands for the particular approach to calculate time-dependent basis set, and "basis" is the size of the underlying time-independent basis set.

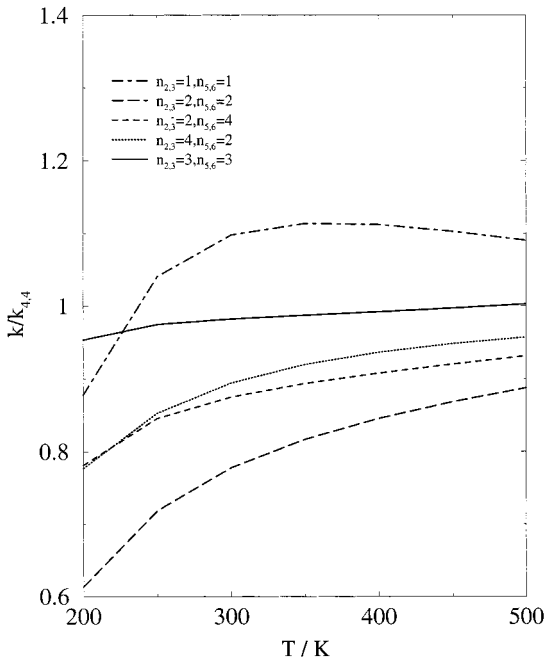

Figure 1. Convergence in the number of single particle functions used to describe the wave function in Q_2,Q_3 and Q_4,Q_5.

(either fast Fourier transform or discrete variable representation on a Hermite basis), the time-independent basis (or grid) on which these are calculated and, when the fast Fourier method is employed, the grid edges. From the table, we notice that most effort is put on the description of wave function in the Q'_1 and Q'_9 coordinates. It is quite clear that it should be so for Q'_1 since it is the reaction coordinate, but in the case of Q'_9 this points out its tight relation with the reaction coordinate.

Since it would be tedious to describe all the details of the convergence procedure, we restrict ourselves to some illustrative examples. Similar tests have been carried out for all degrees of freedom. The particular case of the time dependent basis concerning the low and high-frequency bending modes ($Q_{2,3}$ and $Q_{5,6}$) is presented. These modes are especially interesting since they seem to effect the dynamics of the system. In Figure 1, convergence in the number of single particle functions used on the two doubly degenerate bending modes is shown, by representing the ratio between the rate coefficient for a given time-dependent basis size and the rate constant using four single particle functions in Q_2, Q_3, Q_5, and Q_6. From the figure, it can be seen that three single particle functions for each coordinate ought to be sufficient for the rate to be converged within the temperature range of this work. For this choice there is only a 4% deviation at the lowest temperature with respect to the result using four single particle functions in each mode. The two doubly degenerate bending modes do not seem to be *dynami-*

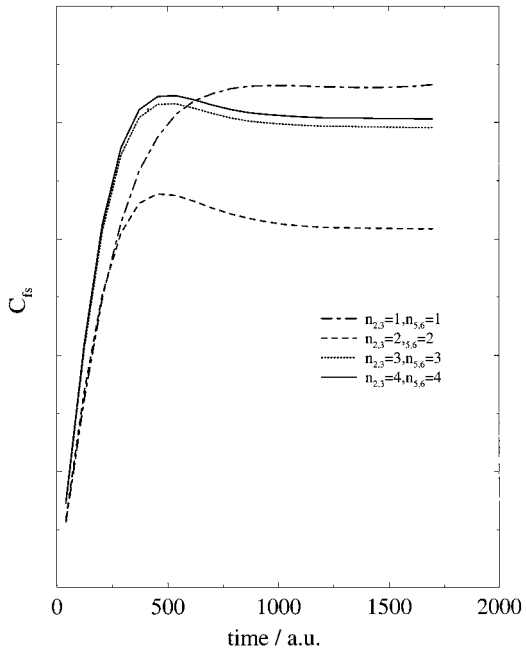

Figure 2. Flux correlation function for several calculations employing a different number of single particle functions used to describe the wave function in Q_2,Q_3 and Q_4,Q_5.

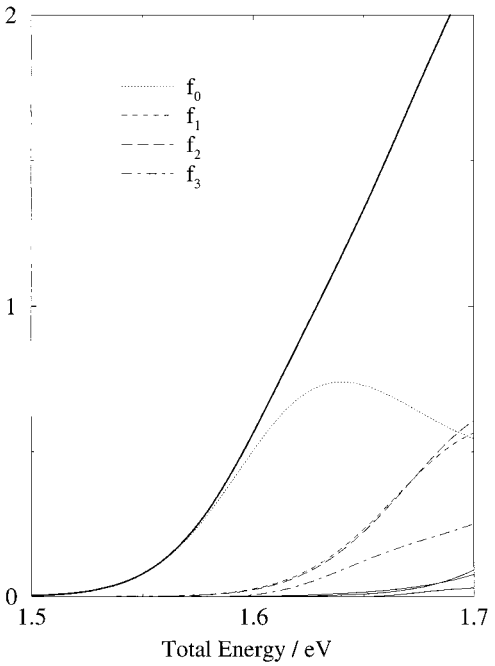

Figure 3. Cumulative reaction probability for $J = 0$ (solid line) and the different flux-eigenstates contributions as a function of energy.

cally different since the curves with $n_{2,3} = 4$, $n_{5,6} = 2$ and $n_{2,3} = 2$, $n_{5,6} = 4$ are quite similar, just a slight difference at high temperature indicates maybe a greater relevance of the lower frequency bending mode due to an excited flux eigenstate whose function shows a node on this coordinate, as it will be shown later.

It is interesting to notice that by employing only one single time-dependent basis function (this would correspond to a straightforward Hartree product) one obtains significantly higher results than the converged ones. Introducing a second single particle function, the values of the rate coefficient decrease noticeably. This can be rationalized by observing Figure 2, where the flux-position correlation function is shown for different sizes of the time-dependent basis employed on these coordinates. In the figure it can be seen how the $n_{2,3} = 1$, $n_{5,6} = 1$ correlation function increases monotonically while the inclusion of an additional basis function lowers the plateau of the curve at long propagation times and introduces some recrossing probably due a greater flexibility of the wave function.

Using the described parameters for the representation of the MCTDH wave function, the cumulative reaction probability has been calculated for zero total angular momentum, $J = 0$, as described in section 2. A reference temperature of 300K has been employed. A propagation time of 40 fs ensures convergence of the flux correlation function. Fourteen iterations in the Lanczos scheme yield 10 converged F_T-eigenstates. This number is sufficient to converge the cumulative reaction probability for energies up to 1.7 eV. These 14 iterations also yield converged rate constant values for temperatures up to 500 K. It should be noted that the calculation of these rate constants includes $N(E)$ values up to 1.85 eV. The $N(E)$ results for energies between 1.7 and 1.85 eV are not converged as accurately as for energies below 1.7 eV. Since these energies yield only a small contribution to $k(T)$, their lesser accuracy has no relevant effect on the accuracy of $k(T)$.

Once we considered our results converged, we performed as well a series of calculations in which only certain degrees of freedom were accurately treated while others were considered in an approximate way. Thus, in the following section reduced dimensionality results will be presented for a series of models considering accurately just three, four, seven, or eight degrees of freedom. In the three-dimensional model (3D), the corresponding degrees of freedom are the reaction coordinate, the umbrella mode, and the a_1 stretching mode mainly involving the vibration of the $H-H-CH_3$ fragments which we have already seen to be strongly related to the reaction coordinate (i.e., Q'_1, Q_4, and Q'_9). In the four-dimensional model (4D), the high frequency a_1 C−H symmetric stretch essentially concerning the CH_3 methyl fragment (Q_{10}) has been added. The seven- (7D) and eight-dimensional (8D) models have been developed from the 3D and 4D ones, respectively, by adding the modes corresponding to the $H-H-CH_3$ bending motion, namely, $Q_{2,3}$ and $Q_{5,6}$. For each of these models, two strategies have been followed concerning the degrees of freedom not accurately included. One has been to *freeze* them completely at their transition state value, $Q = 0$. This has given four models which will be referred to as 3DF, 4DF, 7DF, and 8DF models. Another strategy has been to invoke the time-dependent Hartree approximation, i.e., to use just one single particle function for those degrees of freedom not accurately treated (3DH, 4DH, 7DH, and 8DH models). Concerning the *frozen* models, we find convenient to point out that the corresponding zero point energies and harmonic vibrational partition functions for those degrees of freedom not treated were included in the calculation of the respective rate constants.

IV. Results and Discussion

The converged cumulative reaction probability as a function of total energy (with respect to the $H + CH_4$ asymptote) and the corresponding contributions of the different thermal flux eigenstates (a univocal procedure to define such contributions has been detailed in ref 31) can be seen in Figure 3. Although the ground state (f_0 in Figure 3) accounts for most of the reactivity at temperatures within our working range, the contribution of the two degenerate first excited states, f_1 and f_2, to the system's reactivity is significant at high energy values. These states can be considered first excitations of the low-

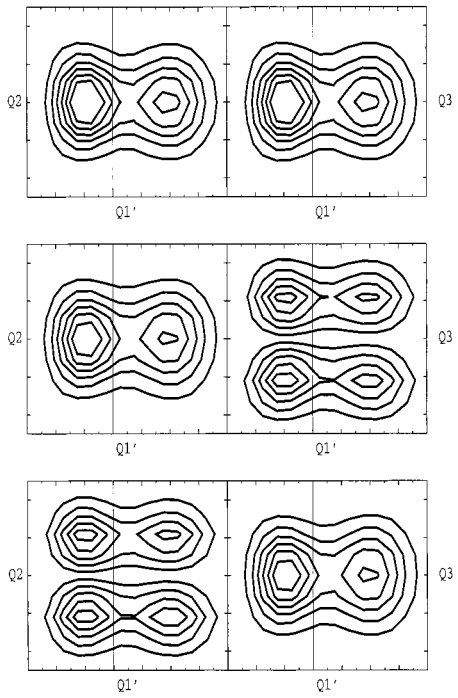

Figure 4. Contour plots of the ground state (f_0, upper part), and first two excited degenerate (f_1, middle, and f_2, lower part) wave packets mapped on the Q_1' and Q_2 coordinates in the corresponding left-hand parts and on the Q_1' and Q_3 coordinates in the right-hand ones. Vertical lines indicate the $Q_1' = 0$ dividing surface.

frequency doubly degenerate bending normal mode of the transition state ($Q_{2,3}$). To check this extent, the ground state and first two excited wave functions have been mapped onto the two-dimensional Q_1',Q_2 and Q_1',Q_3 spaces. The corresponding contour plots are shown in Figure 4 where it can be seen how, while the ground state shows no nodes, the degenerate first two excited states show a node in one of the coordinates, f_1 on Q_3 and f_2 on Q_2. When projecting these states onto the rest of coordinates no additional nodes were found for any of them. The fourth contribution to the cumulative reaction probability in Figure 3, f_3, is somewhat different in nature. The thermal flux eigenstate cannot be associated with a separate vibrational state of the activated complex. It shows the same nodal pattern as f_0 but has a different structure along the reaction coordinate. Thus, f_3 can be viewed as an additional contribution arising from the ground vibrational state.

From the above cumulative reaction probability result for total angular momentum equal zero ($J = 0$) thermal rate constant values were calculated for temperature values between 200 and 500 K employing the J-shifting approximation.[32] The J-shifting scheme can be expected to yield accurate results for the present reaction, since the transition state geometry is well defined and the moments of inertia proved not to change significantly within the range of relevant geometries. Thus, we straightforwardly used the moments of inertia at the transition state (21423, 57370, and 57370 au) in the J-shifting scheme. The corresponding Arrhenius plot is shown in Figure 5 together with experimental results. Theoretical results prove to be much larger than experiment thus suggesting that further improvement on the potential energy surface would be desirable to achieve a better agreement with the experimental points.

As said before, the test of simplified models on complex systems is, to our understanding, a key step in order to get a better feeling of their possible extension to systems of chemical interest. Under this scope, in the same figure, the results of three

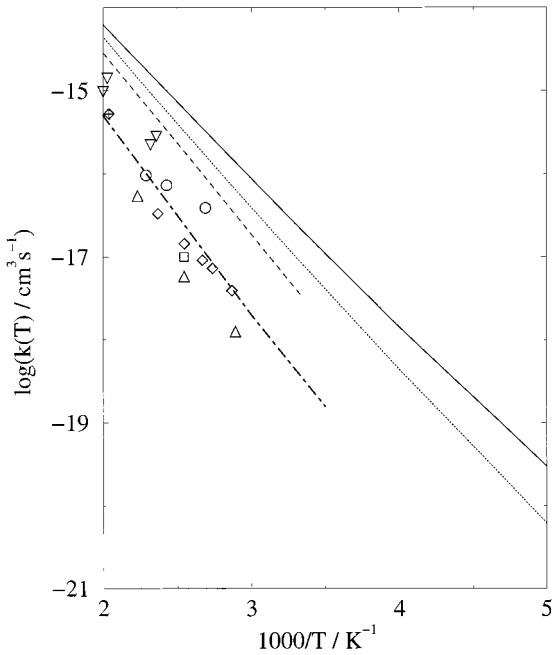

Figure 5. Arrhenius plot for the thermal rate constant. Solid line labels our full-dimensional result, dotted stands for ref 19 (4D-RBU), dashed for ref 18 (3D), and dot−dashed for ref 20 (4D-SVRT) results. Symbols are used for experiment.

relatively recent reduced dimensionality studies[18−20] on the title system are shown. One approach is Takayanagi's three-dimensional model[18] where CH_3 methyl group is considered as a *CX* pseudo-diatomic molecule and the $CH_4 + H \rightarrow CH_3 + H_2$ reaction is treated as a collinear $XCH + H \rightarrow XC + H_2$ process. Another reduced dimensionality approach applied to the title system has been the four-dimensional rotating bond umbrella (RBU) model developed by Nyman and co-workers.[19] In the RBU calculation for $H + CH_4$, the methyl group was again substituted by a CX pseudo-diatom but, unlike the previous model, it is the center of mass of CX and the two hydrogens that lie on a line and, therefore, rotation of the pseudo-diatom is allowed. From observation of the figure, one can see that both reduced dimensionality models do not quite reproduce the full-dimensional curve. The RBU model proves to give significantly better results than the three-dimensional approach of Takayanagi, certainly due to the inclusion of this rotating motion which correlates with the bending normal modes of the transition state that have proven to be relevant in our calculations. Most recently, Wang, Zhang, and Zhang have applied the SVRT model[33] to this system. While this method has given very good agreement with exact quantum results for the $H + H_2O$ reaction, their results seem to be significantly lower than the full-dimensional ones and other approximate approaches for the present case. A number of reasons could explain this deviation of the SVRT rates compared to the accurate ones on the Gilbert-Jordan surface. First, Wang et al. calculate the rate constant only for the rotational and vibrational ground state of methane. They then assume the thermal rate constant to be equal to this state selected rate constant. Second, they freeze the umbrella angle at its transition state value of 107.45°. This modifies the effective reaction barrier on their reduced dimensional surface. The present work indicates that the dynamics in the umbrella angle significantly contributes to the reaction process, so freezing this angle could result in an inadequate description of the whole process.

Although it was already presented in our first communication,[1] for the sake of completeness we include in Table 3 the full-

TABLE 3: Calculated Thermal Rate Constants (k_{QM}, cm^3 s^{-1}) for the Title Reaction[a]

T/K	$k_{QM}(T)$	$k_{TST}(T)$
200	3.00(−20)	9.05(−22)
250	1.45(−18)	1.36(−19)
300	2.19(−17)	3.89(−18)
400	7.35(−16)	2.69(−16)
500	6.19(−15)	3.62(−15)

[a] In the third column transition state theory results (k_{tst}) are added to estimate the relevance of quantum effects in the system

dimensional quantum mechanical results together with the corresponding classical transition state theory ones. Comparison of the numbers given in this table, points out the magnitude of the quantum effects in this system, confirming previous observations.[18−20] As expected, this effect is most noticeable at low temperature where it accounts for almost two orders of magnitude in the rate constant and even at high temperatures where it raises the rate value about a 100%.

As said in the previous section, besides the full-dimensional calculation, a series of reduced dimensionality studies have been carried out considering three, four, seven, and eight degrees of freedom and treating the obviated coordinates either by one single particle function (hereinafter referred to as *Hartree* models) or freezing them at the transition state value (see end of section III). Comparison of these approximate calculations to the exact ones is expected to provide information about the relevance of the different degrees of freedom. In Figures 6a,b the performance of the different reduced dimensionality models, Hartree and frozen, can be found. To make the figures more explicit, we show the deviation of the respective calculated rate constants with respect to the converged 12-dimensional result, k_{12D}. From observation of Figure 6a, comparing the curves corresponding to the three- and seven-dimensional models it can be seen how including the modes corresponding to the H−H−CH_3 bending ($Q_{2,3}$ and $Q_{5,6}$) modifies significantly the system's reactivity. In the plots, one can see how reactivity is not only increased but also the shape of the curve is altered when going from the 3DH model to the 7DH model, or from the 3DF to the 7DF one, this is, when the bending modes are included. The models including the bending motions show a greater reactivity at both low temperature values, probably due to tunneling contributions, and high temperature values, probably due to the contribution of the first two excited thermal flux states which, as seen in Figures 3 and 4 are degenerate and their wave function has a node on the coordinates corresponding to these bending modes. The same comment applies for the four- and eight-dimensional models in Figure 6b.

Another interesting fact can be observed in the same figures when comparing Hartree and frozen models of the same dimensionality. It can clearly be noticed how, just by using a Hartree product function for those degrees of freedom not accurately treated instead of *freezing* them, one obtains a significant improvement of the results. This is even clearer for the more reduced dimensionality models where, treating the bending modes with a single time-dependent function instead of freezing them, makes a big difference (compare 3DF, 3DH in Figure 6a, and 4DF, 4DH in Figure 6b). Moreover, the use of a Hartree model instead of a frozen one does not imply any critical increase of numerical effort. The CPU-time consumed by each model on a single 500 MHz COMPAQ alpha EV6 processor is shown in Table 4. Comparing results in Figure 6a and computation times in Table 4, it turns out that using an inexpensive Hartree-type model as a 3DH, one can get comparable, if not better, results than using a model that includes

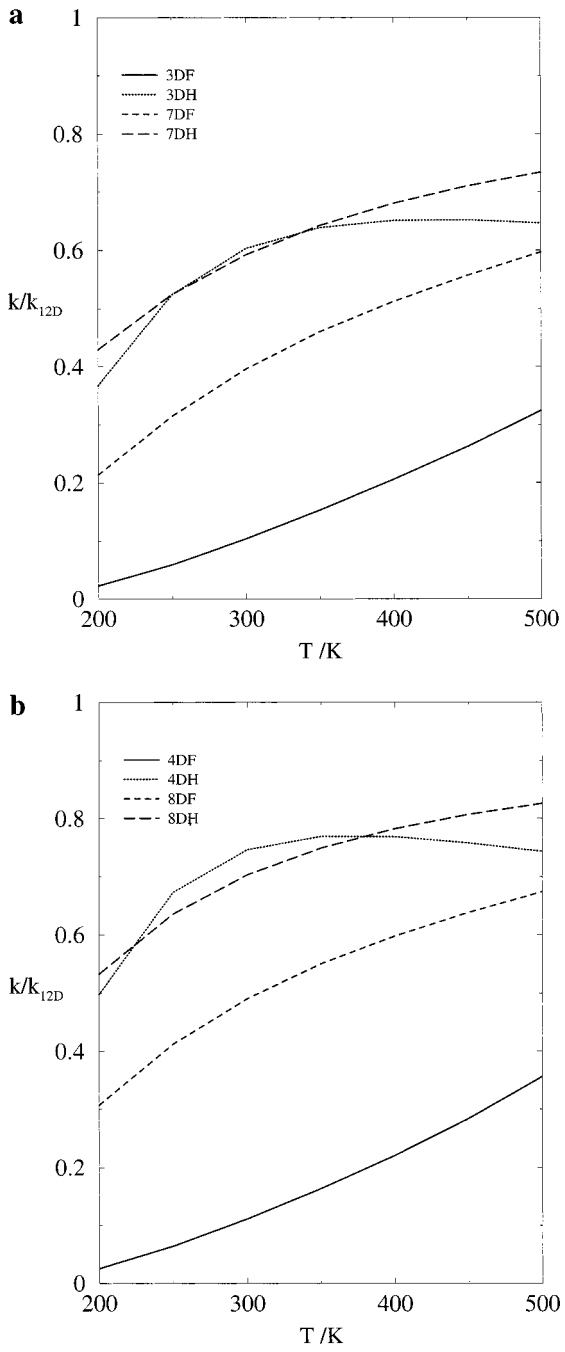

Figure 6. (a) Comparison between three- and seven-dimensional models, both using one single-particle function (3DH, 7DH) and freezing the coordinate (3DF, 7DF). (b) Same as in (a) for four- and eight-dimensional models.

TABLE 4: CPU Time Employed by the Different Reduced Dimensionality Models

	frozen(F)	hartree (H)
3D	5 min	15 min
4D	9 min	27 min
7D	12 h	20 h
8D	26 h	38 h
12D	548 h	

more degrees of freedom but freezes the remaining ones, like the 7DF model (see Figure 6a).

Figure 6a,b can be used as well to investigate the role played by the normal modes which can be essentially assigned to the methyl fragment, namely the a_1 symmetric C−H stretch (Q_{10}), the doubly degenerate bending ($Q_{7,8}$) and the asymmetric doubly

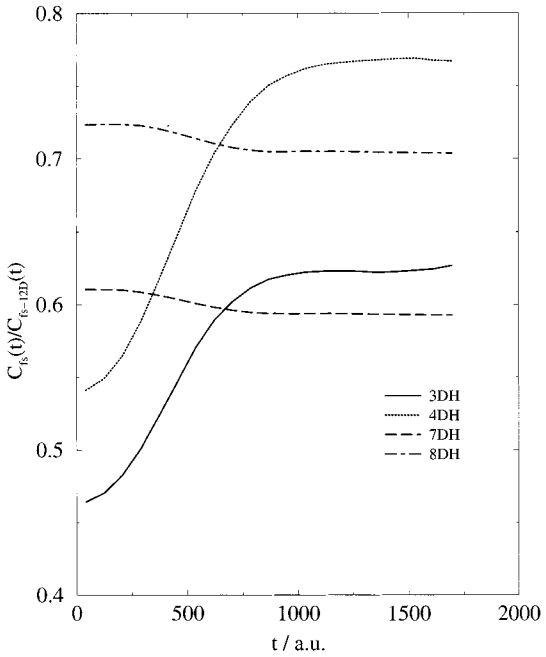

Figure 7. Ratio between the converged flux-position correlation function and those corresponding to the different (Hartree) reduced approximations.

degenerate C−H stretch (Q_{11},Q_{12}). The three- and four-dimensional models, like the seven- and eight-dimensional, differ in the inclusion of the a_1 symmetric C−H stretch of the methyl fragment (Q_{10}). If one compares the performance of the three-dimensional models (Figure 6a) with the four-dimensional ones (Figure 6b), one sees that the 4D curve is shifted upward with respect to the 3D one but it has the same shape. According to this, one could come to the conclusion that this mode does not qualitatively change the dynamics of the process.

To build up a more solid basis for this statement, the flux-position correlation function

$$C_{fs}(t) = tr(\hat{F}_T\, e^{i\hat{H}t/\hbar} h e^{-i\hat{H}t/\hbar}) = \sum_l f_l \langle f_l | e^{i\hat{H}t/\hbar} h e^{-i\hat{H}t/\hbar} | f_l \rangle$$

is investigated for the several models at a temperature of $T = 300$ K. It should be noted that the time dependence of $C_{fs}(t)$ is caused by the evolution of the thermal flux eigenstates while its size depends also on the value of the thermal flux eigenvalues. The relevance in the dynamics of a particular degree of freedom can be estimated in terms of correlation functions by comparing the full-dimensional function to one corresponding to a model where this degree of freedom has been excluded. Following this, the ratio between the different reduced dimensionality flux correlation functions and the accurate one have been plotted in Figure 7. In this figure, it can be observed from the curve corresponding to the 7DH and the 8DH models how excluding the modes corresponding to the methyl fragment from the calculation and treating them with a Hartree function gives an almost constant curve. This means that, with respect to the full-dimensional correlation function, only the eigenvalues of the thermal flux operator vary but the time evolution of the thermal flux eigenstates is the same. Therefore, one can conclude that the effect of these degrees of freedom can be viewed as thermodynamical, modifying (improving) the energy of the vibrational state of the activated complex, and not as a *dynamical* effect. This can be further understood comparing the parallel curves corresponding to the 7DH and 8DH models, which only differ in the $C - H$ methyl symmetric stretch Q_{10}, the system's evolution is the same, only the initial state is better described. On the other hand, observing the variation in the curve corresponding to the 3DH model in Figure 7, mostly between 0 and 1000 au of time, the qualitatively important role played in the dynamics by the H−H−CH_3 bending modes can be further proven.

V. Conclusions

In brief, full-dimensional quantum mechanical results have been reported for the hexa-atomic $CH_4 + H \rightarrow CH_3 + H_2$ reactive process. Under this frame, the system shows a remarkable quantum effect confirming previous reports. However, full-dimensional quantum mechanical results for the rate constant fail to reproduced the experiment, for which further improvement of the potential energy surface ought to be accomplished. Comparison to previously published approximate results on the title system reveals an underestimation of reactivity by these approaches probably attributable to their dimension restrictions.

A series of simple reduced dimensionality calculations have been employed in this work to investigate the role played by the different degrees of freedom in the dynamics of the process. From this study, it has been seen that the three degrees of freedom mainly involved in the reaction are the reaction coordinate, the umbrella mode and the a_1 symmetric stretch of the H−H−CH_3 fragments. Besides these, the degrees of freedom corresponding to the H−H−CH_3 bending normal modes in the transition state (and asymptotically correlating to CH_3 rotation, CH_4 bending and rotation) have a nonnegligible relevance in the system's dynamics. On the other hand, it has been seen how those degrees of freedom corresponding to normal modes of the transition state essentially associated with the methyl fragment vibration do influence the value of the rate constant but do not qualitatively alter the underlying dynamics.

Last, it has been proven how fairly good results can be achieved at a low computational cost using a time-dependent Hartree approximation for the less important degrees of freedom.

Acknowledgment. G. Nyman is thanked for providing the rate coefficients for the reduced dimensionality studies. Financial support by the *Deutsche Forschungsgemeinschaft* and by the European Commission through the RTN Program (HPRN-CT-1999-00007) is gratefully acknowledged.

References and Notes

(1) Huarte-Larrañaga, F.; Manthe, U. *J. Chem. Phys.* **2000**, *113*, 5115.
(2) Berlie, D.; LeRoy, D. *Can. J. Chem.* **1954**, *32*, 650.
(3) Baulch, D.; Cobos, C.; Cox, R.; Esser, P. F. C.; Just, T.; Kerr, J.; Pilling, M.; Troe, J.; Walker, R.; Warnatz, J. *J. Chem. Phys. Ref. Data* **1992**, *21*, 411.
(4) Rabinowitz, M.; Sutherland, J.; Patterson, P.; Klemm, R. *J. Phys. Chem.* **1991**, *95*, 674.
(5) Knyazev, V.; Bencsura, A.; Stoliarov, S.; Slagle, I. *J. Phys. Chem.* **1996**, *100*, 11346.
(6) Baeck, H.; Shin, K. *J. Phys. Chem.* **1995**, *99*, 15925.
(7) Momose, T.; Hoshina, H.; Sogoshi, N.; Katsuki, H.; Wakabayashi, T.; Shida, T. *J. Chem. Phys.* **1998**, *108*, 7334.
(8) Walch, S. *J. Chem. Phys.* **1980**, *72*, 4932.
(9) Schatz, G.; Wagner, A.; T. D. Jr. *J. Phys. Chem.* **1984**, *88*, 221.
(10) Bunker, D.; Pattengrill, M. *J. Chem. Phys.* **1970**, *53*, 3041.
(11) Valencich, T.; Bunker, D. *J. Chem. Phys.* **1974**, *61*, 21.
(12) Chapman, S.; Bunker, D. *J. Chem. Phys.* **1975**, *62*, 2890.
(13) Raff, L. *J. Chem. Phys.* **1974**, *60*, 2220.
(14) Steckler, R.; Dykema, K.; Brown, F.; Hancock, G.; Truhlar, D.; Valencich, T. *J. Chem. Phys.* **1987**, *87*, 7024.
(15) Joseph, T.; Steckler, R.; Truhlar, D. *J. Chem. Phys.* **1987**, *87*, 7036.
(16) Duchovic, R.; Hase, W.; Schlegel, H. *J. Phys. Chem.* **1984**, *88*, 1339.

(17) Jordan, M.; Gilbert, R. *J. Chem. Phys*. **1995**, *102*, 5669.
(18) Takayanagi, T. *J. Chem. Phys*. **1996**, *104*, 2237.
(19) Yu, H.-G.; Nyman, G. *J. Chem. Phys*. **1999**, *111*, 3508.
(20) Wang, M.; Li, Y.; Zhang, J.; Zhang, D. *J. Chem. Phys*. **2000**, *113*, 1802.
(21) Miller, W. H. *J. Chem. Phys*. **1974**, *61*, 1823.
(22) Miller, W. H.; Schwartz, S. D.; Tromp, J. W. *J. Chem. Phys*. **1983**, *79*, 4889.
(23) Matzkies, F.; Manthe, U. *J. Chem. Phys*. **1998**, *108*, 4828.
(24) Manthe, U. *J. Chem. Phys*. **1995**, *102*, 9205.
(25) Matzkies, F.; Manthe, U. *J. Chem. Phys*. **1997**, *106*, 2646.
(26) Meyer, H.-D.; Manthe, U.; Cederbaum, L. S. *Chem. Phys. Lett*. **1990**, *165*, 73.
(27) Manthe, U.; Meyer, H.-D.; Cederbaum, L. S. *J. Chem. Phys*. **1992**, *97*, 3199.
(28) Manthe, U.; Matzkies, F. *Chem. Phys. Lett*. **1996**, *252*, 7.
(29) Manthe, U. *J. Chem. Phys*. **1996**, *105*, 6989.
(30) Espinosa-Garcia, J.; García-Bernáldez, *J. Phys. Chem. Phys*. **2000**, *2*, 2345.
(31) Manthe, U.; Matzkies, F. *Chem. Phys. Lett*. **1998**, *282*, 442.
(32) Bowman, J. M. *J. Phys. Chem*. **1991**, *95*, 4960.
(33) Zhang, J. *J. Chem. Phys*. **1999**, *111*, 3929.